Desalination 608 (2025) 118842

Contents lists available at ScienceDirect

Desalination

journal homepage: www.elsevier.com/locate/desal

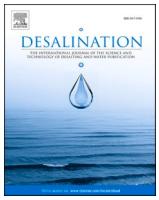

Dual-functional tight ultrafiltration membrane constructed from aminoquinone networks for sufficient dye/salt selectivity and bacterial inactivation☆

Riri Liu [a], Hanna Vanermen [a], Jiale Du [a], Qin Chen [a], Zijian Yu [b], Junwei Li [a], Pengrui Jin [a], Junfeng Zheng [c], Alexander Volodin [d], Wenyuan Ye [e], Raf Dewil [f,g], Ming Xie [h], Jiuyang Lin [i,*], Bart Van der Bruggen [a,*]

[a] Department of Chemical Engineering, KU Leuven, Celestijnenlaan 200F, B-3001 Leuven, Belgium
[b] Materials & Process Engineering (iMMC-IMAP), Université Catholique de Louvain, Place Sainte Barbe 2, 1348 Louvain-la-Neuve, Belgium
[c] School of Carbon Neutrality Future Technology, Sichuan University, Chengdu 610065, China
[d] Department of Physics and Astronomy, KU Leuven, Celestijnenlaan 200D, B-3001 Leuven, Belgium
[e] Jiangxi Provincial Key Laboratory of Water Ecological Conservation at Headwater Regions, Jiangxi University of Science and Technology, 1958 Ke-jia Road, Ganzhou 341000, China
[f] Department of Chemical Engineering, Process and Environmental Technology Lab, KU Leuven, J. De Nayerlaan 5, 2860 Sint-Katelijne-Waver, Belgium
[g] Department of Engineering Science, University of Oxford, Oxford OX1 3PJ, United Kingdom
[h] Department of Chemical Engineering, University of Bath, Bath BA2 7AY, United Kingdom
[i] Key Laboratory of Rare Earths, Ganjiang Innovation Academy, Chinese Academy of Sciences, Ganzhou 341119, China

HIGHLIGHTS

- VA/ε-pl composite network is constructed to design tight ultrafiltration (TUF) membranes.
- TUF membrane with 3450 Da MWCO yields 98.50 % dye rejection and 3.56 % NaCl rejection.
- TUF membrane demonstrates a competitive long-term stability.
- VA/ε-pl composite coating guarantees excellent antimicrobial properties.

GRAPHICAL ABSTRACT

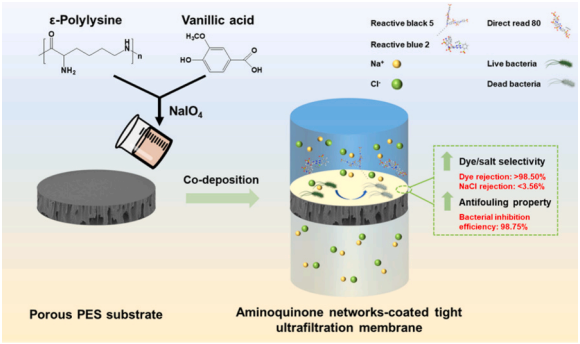

ARTICLE INFO

Keywords:
Highly saline textile wastewater
Tight ultrafiltration membranes
Aminoquinone networks

ABSTRACT

Membranes used for the treatment of highly saline textile wastewater generally suffer from low dye/salt selectivity and biofouling issues. Herein, the facile assembly of vanillic acid/ε-polylysine-based aminoquinone networks (AQN) on a porous PES substrate is proposed for the construction of a dual-functional tight ultrafiltration membrane with high dye/salt separation efficacy and superior antimicrobial functionality. By regulating the

☆ This article is part of a Special issue entitled: 'Desalination technology' published in Desalination.

* Corresponding authors.
E-mail addresses: jylin@gia.cas.cn (J. Lin), bart.vanderbruggen@kuleuven.be (B. Van der Bruggen).

https://doi.org/10.1016/j.desal.2025.118842
Received 28 December 2024; Received in revised form 18 February 2025; Accepted 22 March 2025
Available online 27 March 2025

Dye/salt fractionation
Antimicrobial properties

assembly duration, the surface structure and properties (i.e., thickness, roughness, hydrophilicity and pore size) of the composite AQN coating can be precisely tailored. Specifically, the optimized AQN-60 tight ultrafiltration composite membrane (MWCO of 3450 Da) experienced >98.50 % dye rejection and <3.56 % NaCl rejection for various dye/salt mixtures. Additionally, the prepared AQN-60 composite membrane demonstrated stable fractionation performance with an eventual dye rejection of 98.70 % and salt rejection of 3.98 % after 24-h filtration of a reactive blue 2/NaCl mixed solution. Furthermore, the integration of ε-polylysine onto the AQN-60 composite membrane markedly enhanced the antimicrobial ability of the tight ultrafiltration membrane, which showed good inhibition efficiency (98.75 %) against *E. coli* bacteria.

1. Introduction

The large-scale discharge of dye-laden effluents from the textile industry has become a critical global environmental concern because of the profound ecological and public health risks posed by their toxic and recalcitrant constituents [1–5]. Most conventional remediation approaches for textile wastewater are predominantly treatment oriented, focusing merely on contaminant removal/degradation without resource recovery. However, to achieve environmental sustainability, the organic dyes and inorganic salts present in textile wastewater should be recovered through effective separation processes [6–11].

Pressure-driven membrane technologies, such as loose nanofiltration and tight ultrafiltration, have emerged as promising strategies for dye/salt fractionation due to their high selectivity, operational simplicity, and low energy input [12–18]. In particular, tight ultrafiltration membranes with moderately appropriate pore sizes (MWCOs of 1000–5000 Da) as competitive alternatives enable efficient dye/salt fractionation, allowing for increased ion transmission and sufficient dye retention at relatively low pressures. Currently, dedicated efforts have been made to explore the practicability of tight ultrafiltration membranes for dye/salt fractionation. For example, Lin et al. evaluated the commercial tight ultrafiltration membrane UH004 (MWCO of 4700 Da) for dye/salt separation, which achieved over 98.9 % dye retention with high salt permeation (<2.0 %) [19]. Ye et al. developed tight ultrafiltration membranes with MWCOs of 1000–5000 Da through the co-deposition of polydopamine/polyethyleneimine triggered by ammonium persulfate [20]. The optimal membrane (MWCO of 1700 Da) exhibited >98.2 % rejection for reactive dyes (molecular weights of 610–1000 Da) with >97.0 % NaCl permeation. Hu et al. prepared a PES/SPSf tight ultrafiltration membrane via non-solvent induced phase separation using adipic acid as an additive. The resulting membrane, with an MWCO of 7250 Da and an average pore size of 1.8 nm, displayed satisfactory dye/salt separation (92.1 % AB25 dye retention and 8.0 % NaCl retention) with a permeance flux of 37.6 $L{\cdot}m^{-2}{\cdot}h^{-1}{\cdot}bar^{-1}$ [21].

Despite the substantial development of tight ultrafiltration membranes, currently available membranes are still prone to significant fouling due to their inherently poor hydrophilicity [22–24]. Moreover, because of the limited antibacterial activity of these membranes, their separation performance is remarkably compromised by microorganism-induced biofouling [25]. Therefore, engineering highly anti-biofouling tight ultrafiltration membranes has become a critical priority. Wu et al. designed an anti-biofouling membrane via in situ photografting of polyhexamethylene biguanide and polyethylene glycol on a photoreactive polyamide layer, which achieved a permeance flux of 18.6 $L{\cdot}m^{-2}{\cdot}h^{-1}{\cdot}bar^{-1}$ with 98.6 % bacterial inhibition [26]. Qu et al. reported an electrically conductive anti-fouling membrane prepared by the deposition of quaternary ammonium compounds and pyrrole composites onto a PVDF substrate [27]. The modified membranes exhibited complete bacterial inactivation, leading to a >20 % increase in the final normalized water flux.

Various strategies have been developed to construct fouling-resistant surfaces, among which the integration of hydrophilic and antibacterial materials onto the substrate surface via surface deposition stands out as a simple and feasible approach [28]. Recently, bioinspired substrate-independent aminoquinone networks have garnered widespread attention, as they provide a versatile platform for the precise design of multifunctional coatings with well-defined properties and structures (e.g., surface wetting, surface charges and thickness) [29–33]. Inspired by these remarkable properties, the synergistic integration of AQN coatings and antimicrobial monomers to fabricate antifouling tight ultrafiltration membranes represents a promising approach. In this context, ε-polylysine, a natural antimicrobial polypeptide with a structure rich in amino groups, has been demonstrated to be an ideal amino monomer candidate for improving the hydrophilicity and antibacterial properties of substrates [34–36].

In this study, dual-functional tight ultrafiltration membranes with high dye/salt selectivity and antibacterial properties were developed through the co-assembly of aminoquinone networks (vanillic acid-based quinone and ε-polylysine) on a porous PES ultrafiltration membrane substrate. The selective layer properties, i.e., thickness, roughness, hydrophilicity and pore size distribution, were tailored by adjusting the co-assembly durations of the aminoquinone networks. In addition, filtration performance tests, including separation efficiency and long-term stability tests, were conducted to evaluate the robustness of the fabricated tight ultrafiltration membranes for dye/NaCl fractionation. Furthermore, the antimicrobial performance of the fabricated composite tight ultrafiltration membranes was investigated by assessing their inhibition efficacy against *E. coli*. This study offers a promising strategy for fabricating aminoquinone networks-based dual-functional tight ultrafiltration membranes for the sustainable management of textile wastewater, addressing both resource recovery and zero liquid discharge.

2. Experimental

2.1. Chemicals and materials

A polyethersulfone (PES) ultrafiltration membrane with an MWCO of 50 kDa was selected as the porous substrate. Vanillic acid (VA, Sigma-Aldrich, Belgium), sodium periodate ($NaIO_4$, Sigma-Aldrich, Belgium) and ε-polylysine (ε-pl, Handary Co., Ltd., Belgium) were utilized in surface deposition to construct aminoquinone networks. Sodium chloride (NaCl), reactive blue 2 (M_w = 774.2 $g{\cdot}mol^{-1}$), reactive black 5 (M_w = 991.8 $g{\cdot}mol^{-1}$) and direct red 80 (M_w = 1373.1 $g{\cdot}mol^{-1}$), supplied by Sigma-Aldrich (Belgium), were employed for the membrane filtration tests. Polyethylene glycol polymers (PEGs, Sigma-Aldrich, Belgium) with molecular weights of 600, 1500, 3000, 6000 and 10,000 Da were used to determine the MWCOs of the prepared tight ultrafiltration membranes. Unless otherwise specified, all reagents were used as received. Deionized water was utilized throughout all the experiments.

2.2. Preparation of the AQN-coated tight ultrafiltration membranes

Tight ultrafiltration membranes were fabricated through the co-deposition of vanillic acid and ε-polylysine with sodium periodate as an oxidizing agent (Fig. 1). Specifically, vanillic acid (2.0 $g{\cdot}L^{-1}$), sodium periodate ($NaIO_4$, 0.2 $g{\cdot}L^{-1}$) and ε-polylysine (2.0 $g{\cdot}L^{-1}$) were sequentially dissolved in 20 mL of deionized water and homogenized by ultrasonication to prepare the modification solution. The porous PES substrate was positioned in a custom-designed modification mold, after which the as-prepared modification solution was applied to the

substrate surface to initiate the deposition process. To ensure uniform co-deposition, the mold was placed in a shaker set at 75 rpm for varying co-deposition durations (15, 30, 60, 90, and 120 min). The modified membrane was then rinsed multiple times with deionized water to remove any residual chemicals. All the membranes were stored in deionized water at 4 °C before use. The resulting membranes were designated AQN-15, AQN-30, AQN-60, AQN-90, and AQN-120, corresponding to co-deposition durations of 15, 30, 60, 90, and 120 min, respectively.

2.3. Characterization

A systematic characterization was carried out to investigate the synthesized AQN-based tight ultrafiltration membranes. Fourier transform infrared spectroscopy (FT-IR, PerkinElmer Spectrum 100, Germany) and X-ray photoelectron spectroscopy (XPS, monochromatic aluminum Kα, Thermo Scientific, America) were employed to analyze the chemical compositions of the prepared membranes. The detailed surface and cross-sectional morphologies of the formed AQN coating were visualized via a scanning electron microscope (SEM, XL30 FEG, Netherlands) operating at 10 kV. To enhance signal quality and improve imaging resolution, the membrane samples were sputter-coated with a thin layer of gold nanoparticles prior to SEM imaging. Atomic force microscopy (AFM, Dimension 3100D, Bruker, USA) was used for quantitative analysis of surface roughness. Measurements were performed in tapping mode using PPP-NCHR probes (NanoAndMore GmbH) with a spring constant of 40–50 N/m and a nominal tip apex radius of <7 nm. A contact angle goniometer (OCA 20, Dataphysics Instruments, Germany) was used to assess the surface hydrophilicity of the membranes. All the membrane samples were dried at room temperature before characterization.

2.4. Membrane performance evaluation

The filtration performance of the fabricated AQN-coated composite membranes was assessed by using a custom cross-flow filtration setup with an effective area of 7.0 cm^2. Prior to testing, the membrane was pre-compacted at 4 bar for at least 30 min. Water permeance was then measured by recording the collected permeate volume during a fixed filtration time, as described by Eq. 1:

$$J_p = \frac{V}{A \times \Delta t \times P} \quad (1)$$

where V is the volume of the permeate collected during a fixed filtration interval of Δt; A is the effective filtration area; and P is the applied operating pressure.

The rejection of the membranes was examined via single-component NaCl solutions of various concentrations (0.1, 0.5, 2.0 and 10.0 $g{\cdot}L^{-1}$) and pure dye solutions (reactive blue 2, reactive black 5 and direct red 80) at a concentration of 0.2 $g{\cdot}L^{-1}$. Moreover, both a reactive blue 2/NaCl mixture and a reactive black 5/NaCl mixture with varying NaCl concentrations (i.e., 1.0, 2.0, 5.0 and 10.0 $g{\cdot}L^{-1}$) were prepared to evaluate the separation performance of the fabricated AQN-coated tight ultrafiltration membranes. Furthermore, continuous 24-h filtration of a reactive blue 2/NaCl mixture (0.2 $g{\cdot}L^{-1}$ dye; 5.0 $g{\cdot}L^{-1}$ NaCl) was carried out to evaluate the long-term stability of the AQN-coated tight ultrafiltration membranes. All the membrane performance tests were conducted at an operating pressure of 4 bar. Solute rejections (R) were calculated via Eq. 2:

$$R = \left(1 - \frac{C_p}{C_f}\right) \times 100\ \% \quad (2)$$

where C_p and C_f are the solute concentrations in the permeate solution and feed solution, respectively.

The selectivity (S) between the dye and NaCl was calculated via Eq. 3:

$$S = \frac{1 - R_{NaCl}}{1 - R_{dye}} \quad (3)$$

where R_{NaCl} and R_{dye} represent the NaCl rejection and dye rejection of the membrane in the separation of the dye/salt mixture, respectively.

The normalized flux during 24-h long-term operation was determined via Eq. 4:

$$Normalize\ flux = \frac{J_{final}}{J_{initial}} \times 100\ \% \quad (4)$$

where J_{final} and $J_{initial}$ are the final and initial permeance, respectively.

2.5. Molecular weight cutoff (MWCO) measurements

The MWCOs of the AQN-coated composite membranes were determined via a feed mixture containing 0.2 $g{\cdot}L^{-1}$ PEGs with mean molecular weights ranging from 600 to 10,000 Da at 25 °C and an operating pressure of 4 bar. The rejection of PEGs was calculated via Eq. 5:

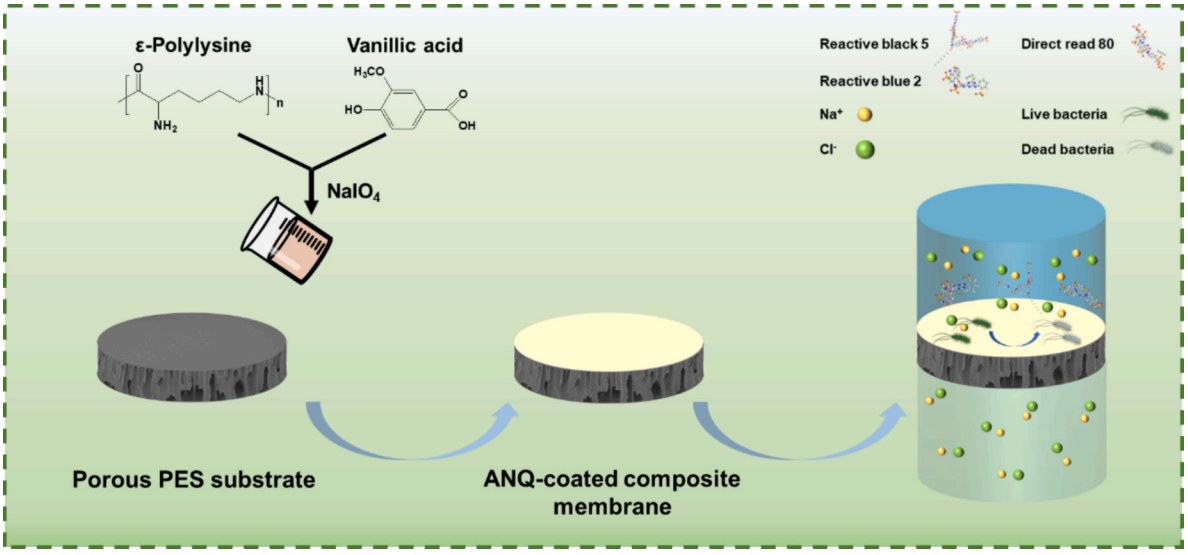

Fig. 1. Schematic diagram of the preparation of the AQN-coated tight ultrafiltration membranes.

$$R_{PEG} = \left(1 - \frac{C_{PEG,permeate}}{C_{PEG,feed}}\right) \times 100\ \% \quad (5)$$

where $C_{PEG,\ feed}$ and $C_{PEG,\ permeate}$ are the concentrations of PEG polymers in the feed and permeate solutions, respectively, which were determined via a total organic carbon analyzer (TOC, ASI-5000 A, Japan).

The Stokes diameter of the PEGs (d_s) was calculated via Eq. 6:

$$d_s = 33.46 \times 10^{-12} \times MW^{0.557} \quad (6)$$

where MW represents the molecular weight of the PEGs.

The pore size distribution of the membrane was derived from the log-normal probability function describing the relationship between the R_{PEG} and d_p (Eq. 7).

$$\frac{dR(d_p)}{dd_p} = \frac{1}{d_p ln\sigma_p \sqrt{2\pi}} exp\left[-\frac{\left(lnd_p - ln\mu_p\right)^2}{2\left(ln\sigma_p\right)^2}\right] \quad (7)$$

where μ_p is the mean effective pore size of the membranes, determined at $R_{PEG} = 50$ %, and σ_p is the geometric standard deviation, calculated as the ratio between d_p at an R_{PEG} of 84.13 % and μ_p. The MWCO value was obtained as the molecular weight of the PEGs at which the rejection reached 90 %.

2.6. Antibacterial test

The antibacterial efficacy of the prepared AQN-coated composite membranes was evaluated via standard plate counting protocols. Specifically, membrane samples with dimensions of 2 cm × 3 cm were immersed in 6 mL of *E. coli* suspensions and shaken for 12 h at 30 °C. After the antibacterial process, the bacterial suspensions were serially diluted and inoculated onto LB agar plates. The plates were incubated at 37 °C for 12 h, after which colony counts were performed to assess bacterial growth. The *E. coli* inhibition efficiency (N) of the AQN-coated tight ultrafiltration membranes was determined via Eq. 8:

$$N = \left(1 - \frac{Q_t}{Q_0}\right) \times 100\ \% \quad (8)$$

where Q_0 and Q_t represent the quantity of plate colonies without and with the AQN-coated tight ultrafiltration membrane, respectively.

3. Results and discussion

3.1. Role of $NaIO_4$ in the kinetics of VA/ε-pl composite aminoquinone networks

The kinetics of aminoquinone networks are significantly influenced by solution conditions, particularly the presence of oxidants. To investigate the role of $NaIO_4$ in the formation of VA/ε-pl composite aminoquinone networks, two distinct modification solutions were prepared:

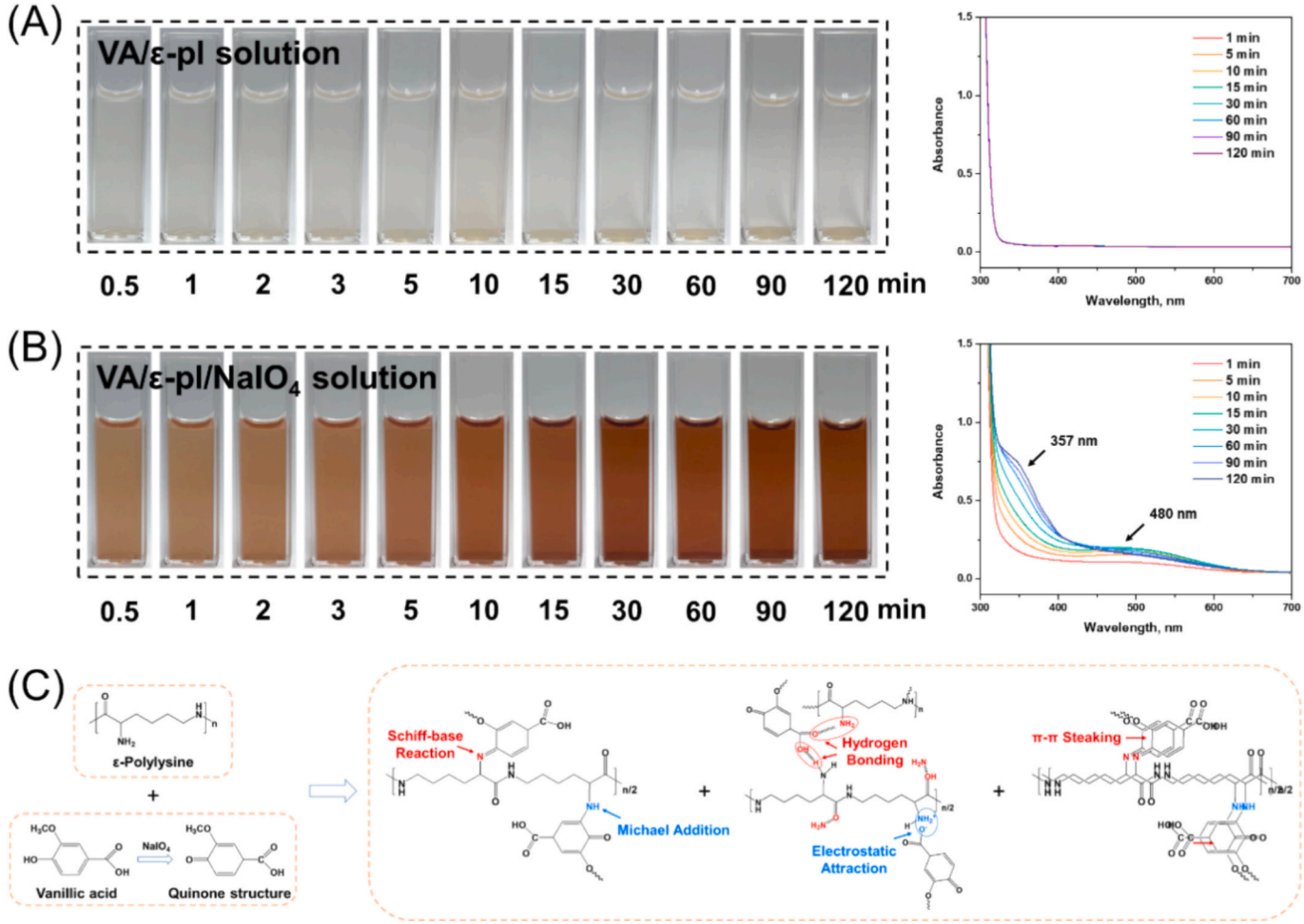

Fig. 2. Color evolution and UV–vis absorbance profiles of vanillic acid/ε-polylysine solutions with (A) and without (B) $NaIO_4$ during 120 min co-deposition; (C) The possible reaction mechanism for the formation of aminoquinone networks.

one containing $NaIO_4$ and the other serving as a control without $NaIO_4$. Over a 120-min reaction duration, a pronounced difference in the visual appearance of the solutions was observed (Fig. 2). Specifically, the $NaIO_4$-containing solution gradually turned brown, whereas the VA/ε-pl solution remained largely unchanged, indicating that $NaIO_4$ was crucial for initiating the oxidation of vanillic acid to the quinone structure. To further analyze the reaction kinetics and chemical transformations, UV–vis absorption spectra were monitored for both solutions at different time intervals. As shown in Fig. 2A and B, the solution with the addition of $NaIO_4$ displayed two absorption peaks at 357 nm and 480 nm. The peak at a wavelength of 357 nm corresponded to the formation of the quinone structure, suggesting the successful oxidation of vanillic acid by $NaIO_4$ [37,38]. In contrast, no such peak was observed for the control solution, confirming that the absence of $NaIO_4$ significantly hindered the evolution of VA/ε-pl composite aminoquinone networks. Furthermore, the absorption peak at a wavelength of 480 nm resulted from the interaction between the quinone and the amino groups in ε-polylysine through Michael addition and Schiff-base reactions [37]. Michael addition occurs when nucleophilic amine ($-NH_2$) group in ε-polylysine reacts with electrophilic quinone structures, forming the stable C—N covalent bond that enhance the coating stability and resistance to hydrolysis. Additionally, Schiff-base interaction between quinone-derived carbonyl groups and primary amine in ε-polylysine simultaneously generates the C═N bond, which guarantees a stable and highly cross-linked network. In addition, the proposed reaction mechanism between vanillic acid and ε-polylysine for membrane fabrication is illustrated in Fig. 2C. The enhanced UV absorption at both wavelengths of 357 nm and 480 nm with extended reaction times in the $NaIO_4$-triggered solution implied mild and progressive development of aminoquinone networks, which is beneficial for the precise optimization of coating properties.

3.2. Morphologies of the AQN-coated composite membranes

The surface color variation of the AQN-coated membranes is depicted in Fig. 3A. An apparent color shift from brightly white to yellow was observed on the membrane surface upon 15 min of deposition of the VA/ε-pl/$NaIO_4$ mixture, indicating the successful coating of aminoquinone networks onto the substrate. However, the early-stage complex coating appeared in an uneven manner, as evidenced by the irregular color distribution on the membrane surface at short coating durations (e.g., 15 min and 30 min). As the deposition duration increased to 60 min, the intensity and uniformity of the coating coloration improved markedly. The AQN-60 composite membrane yielded a consistent and well-developed yellow color pattern, which indicated thorough co-deposition and sufficient formation of aminoquinone networks on the substrate.

SEM and AFM analyses revealed the detailed microstructural morphology of the VA/ε-pl-based aminoquinone networks (Fig. 3B–G). The pristine PES substrate surface was smooth with a roughness of 1.69 nm. After the co-deposition of the VA/ε-pl/$NaIO_4$ complex, the surface cavity structures became evident, indicating the effective assembly of thin VA/ε-pl composite networks on the PES substrate. The surface roughness of the AQN-coated composite membranes tended to decrease as the co-deposition durations increased. Specifically, the AQN-15 and AQN-30 composite membranes had relatively high roughness values of 4.34 nm and 2.64 nm, respectively, due to the heterogeneous deposition of underdeveloped VA/ε-pl composite aminoquinone networks. In line with the observations in Fig. 3A, the irregular local defects of the AQN composite coating were effectively minimized after sufficient evolution with increasing co-deposition duration, resulting in homogeneous and smooth surfaces with low roughness. In addition, cross-sectional SEM images revealed the effect of deposition duration on the thickness of the coating. Specifically, the membrane thickness increased dramatically to 171 nm within 60 min, demonstrating the rapid cross-linking of the

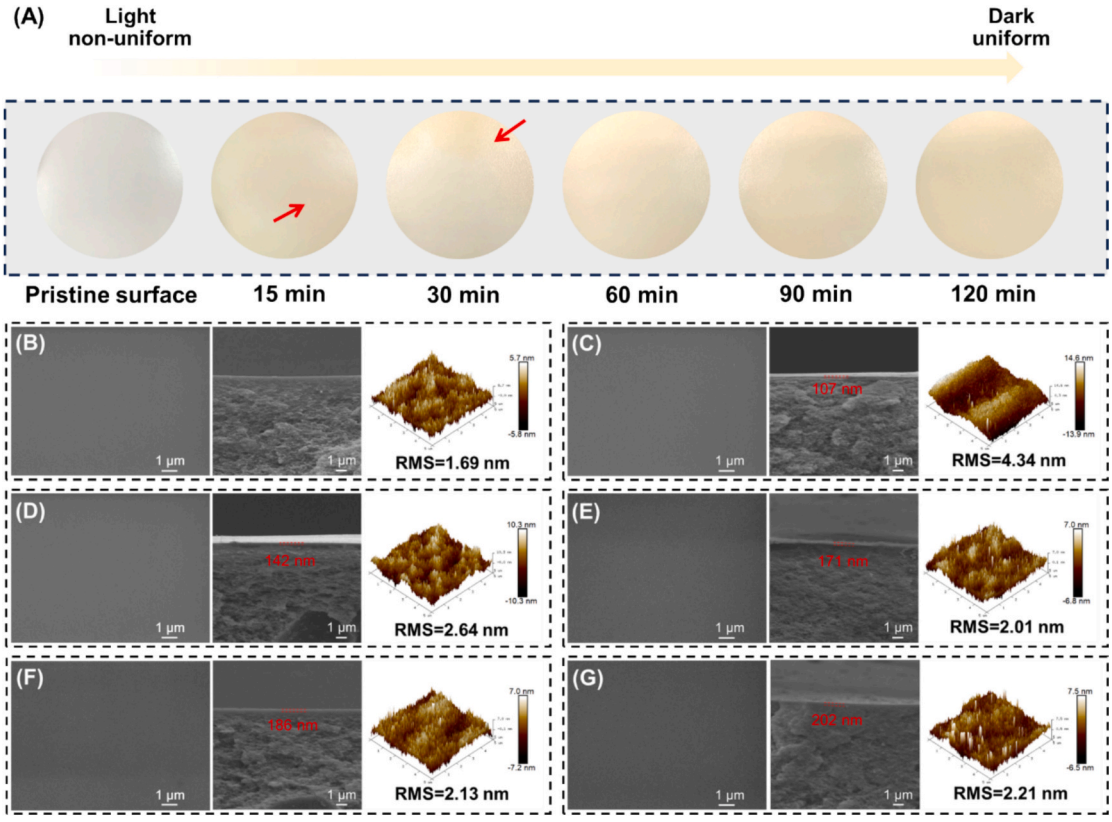

Fig. 3. (A) Photograph of the membrane surface; SEM and AFM characterization of the pristine PES substrate (B), AQN-15 (C), AQN-30 (D), AQN-60 (E), AQN-90 (F) and AQN-120 (G).

aminoquinone networks during the initial stage. Afterwards, the co-deposition kinetics of the composite coating decelerated, and the membrane ultimately reached a thickness of 202 nm (Fig. 3G).

3.3. Chemical composition of the membrane surface

The surface chemical composition of the prepared AQN-coated composite membranes was examined via FTIR and XPS (Fig. 4). As shown in Fig. 4A, two new characteristic peaks were detected at wavenumbers of 1032 and 770 cm^{-1} in the FT-IR spectra of the AQN-coated membranes, which were attributed primarily to the asymmetrical bending vibration of the $–CH_3$ group and the C—H out-of-plane bending of the phenyl groups derived from vanillic acid [39,40]. Additionally, the incorporation of ε-polylysine onto the membrane yielded a typical N—H stretching vibration peak, which can be reflected at the wavenumber of 1520 cm^{-1} in the FTIR spectra of the AQN-coated composite membranes [41]. The incorporation of positively-charged amine groups of not only endowed the membrane with the enhanced hydrophilicity for water penetration, but also induce the electrostatic interactions with negatively-charged bacterial cell membranes for suppression of their proliferation.

The XPS survey spectra (Fig. 4B) revealed that the O 1s and N 1s peaks of the surface-coated membranes increased with increasing evolution duration, which was attributed to the large amounts of O and N derived from vanillic acid and ε-polylysine. Conversely, the percentage of S gradually decreased because of the continuous coating of the composite networks on the membrane surface, which effectively covered the cavity structure of the PES substrate. Importantly, the N 1s narrow scan spectrum of the prepared AQN-coated composite membrane revealed a new peak intensity for the C═N group, which strongly confirmed the covalent interaction of vanillic acid and ε-polylysine via a Schiff-base reaction.

3.4. Surface hydrophilicity

Surface hydrophilicity, a fundamental surface property, determines membrane performance in terms of water permeance and antifouling behavior. The static water contact angles (WCAs) of the pristine PES substrate and the AQN-coated composite membranes are depicted in Fig. 5. As shown in Fig. 5, the virgin surface of the PES substrate yielded moderate hydrophilicity with a WCA of 74.4°. After the coating of the VA/ε-pl aminoquinone networks, the membrane hydrophilicity was markedly enhanced, as evidenced by a substantial reduction in the water contact angle. For example, the AQN-15 composite membrane has a

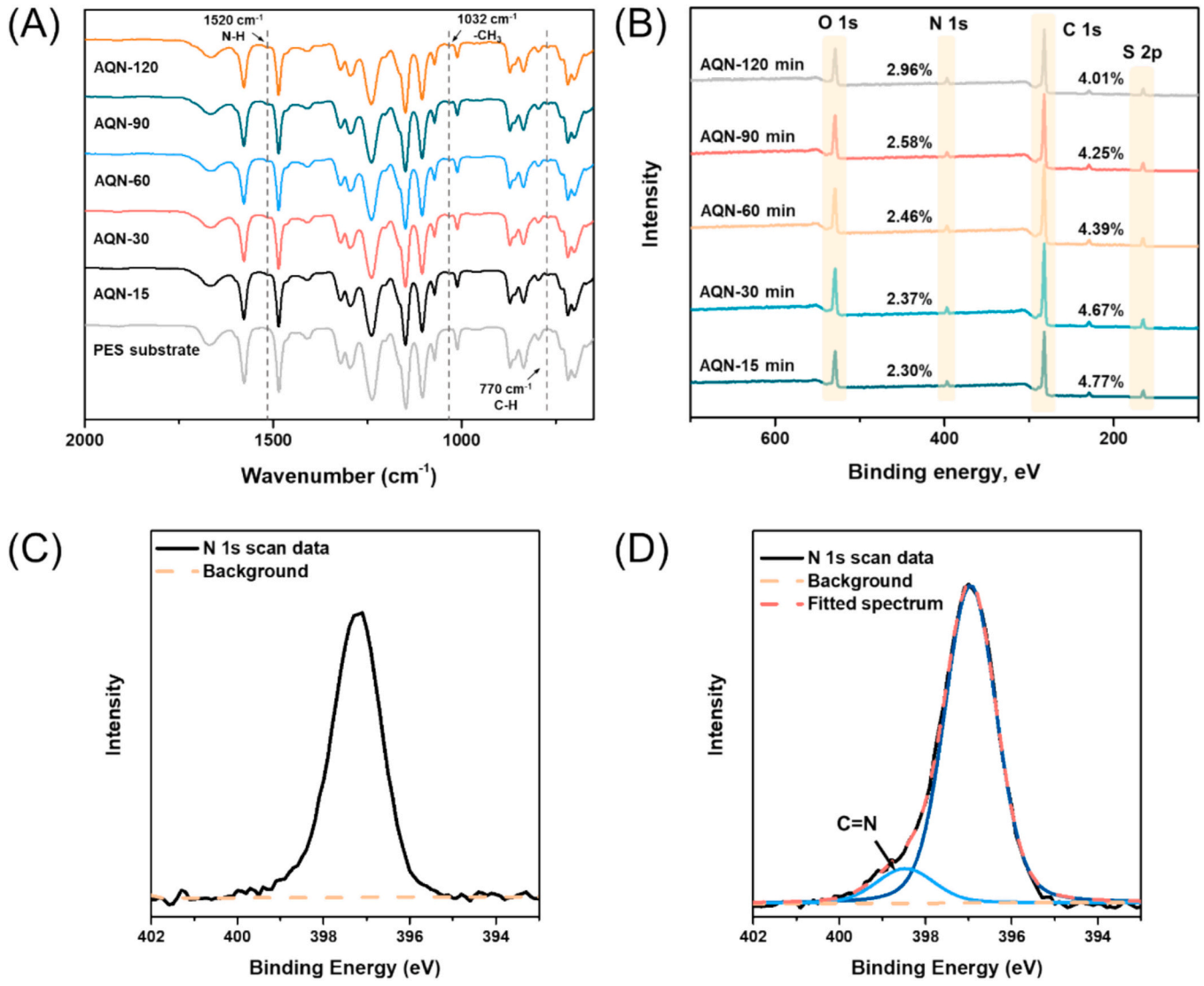

Fig. 4. FT-IR spectra (A) and XPS survey spectra (B) of the AQN-coated composite membranes; N 1s XPS spectra of the PES substrate (C) and AQN-120 composite membrane (D).

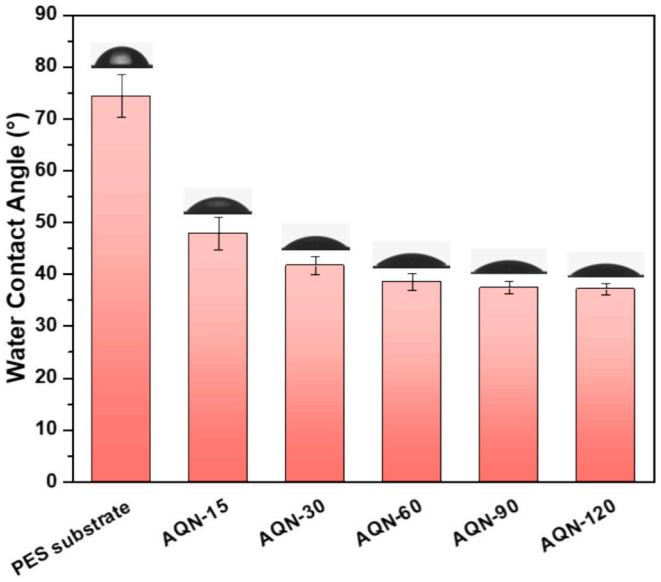

Fig. 5. Water contact angle of the PES substrate and the fabricated membranes as a function of co-deposition duration.

WCA of 47.9° after a 15-min modification. This improved hydrophilicity was due to the integration of hydrophilic functional groups (i.e., amine and carboxyl groups) on aminoquinone networks, which strengthened the surface affinity for water molecules. Additionally, the extension of the deposition duration allowed for further stacking of the hydrophilic-surface layer, consequently lowering the WCA to 37.1°. Therefore, the superior surface hydrophilicity is expected to contribute to high water permeation and robust antifouling performance in long-term sustainable textile wastewater treatment.

3.5. Membrane pore size distribution and MWCO

The MWCO is a key parameter used to characterize the pore size of membranes and is determined by evaluating the rejection of PEGs with different molecular weights. As illustrated in Fig. 6, the porous structure of the PES substrate was effectively covered by the deposition of tight VA/ε-pl composite aminoquinone networks. The resulting AQN-coated composite membranes had a dense surface structure with MWCOs ranging from 3200 to 5970 Da and can be categorized as tight ultrafiltration membranes. It was believed that the reduction in pore size would contribute to an increased rejection of dye molecules, thereby improving the selectivity between the dye and salt.

3.6. Membrane performance evaluation

3.6.1. Filtration performance of the AQN-coated tight ultrafiltration membranes

NaCl solutions with varying concentrations (0.1, 0.5, 2.0 and 10.0 $g{\cdot}L^{-1}$) were prepared to examine the pure salt rejection capacity of the AQN-coated tight ultrafiltration membranes. As presented in Fig. 7A, the water permeance of the membranes decreased from 55.98 to 40.92 $L{\cdot}m^{-2}{\cdot}h^{-1}{\cdot}bar^{-1}$ as the coating duration increased. This decrease in permeance was due to (1) the increase in the selective layer thickness with increasing deposition time extended the water transmission path, thus reducing the permeance, and (2) the progressive decrease in pore size with increasing coating time further hindered water flow, as the narrower pores offered greater resistance to water passage. Fig. 7B depicts the NaCl rejection of the AQN-coated composite membranes at various NaCl concentrations. As expected, the well-developed AQN-coated tight ultrafiltration membranes allowed for greater NaCl retention than did the membranes with shorter coating durations, which was attributed to their compact pore structures with an enhanced size sieving effect. For example, the rejection of a 2.0 $g{\cdot}L^{-1}$ NaCl solution increased noticeably from 3.45 % to 4.98 % as the coating duration increased from 15 min to 120 min. Moreover, increasing the salt concentration enhanced the shielding effect on the membrane surface; therefore, pronounced salt penetration was observed at elevated salinities (e.g., 10 $g{\cdot}L^{-1}$ NaCl).

The permeance of the membranes in different dye solutions (direct red 80, reactive black 5, and reactive blue 2) is presented in Fig. 7C. There was a comparable downward trend in permeance during the filtration of the dye solutions. However, the permeance was slightly reduced due to the small degree of contamination by dye cakes on the surface. In terms of dye rejection (Fig. 7D), the prepared AQN-coated

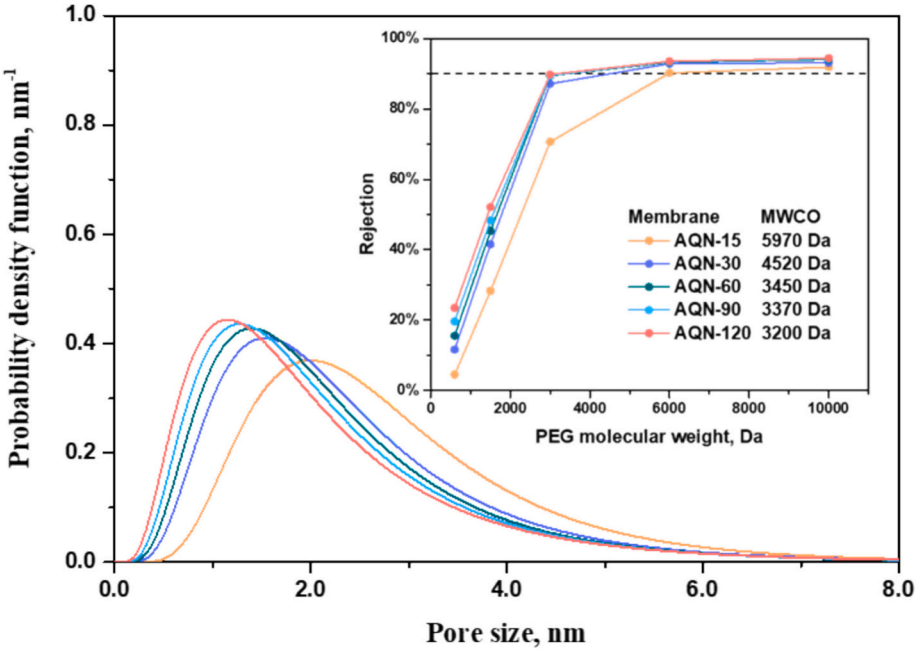

Fig. 6. Pore size distributions and MWCOs of the AQN-coated composite membranes.

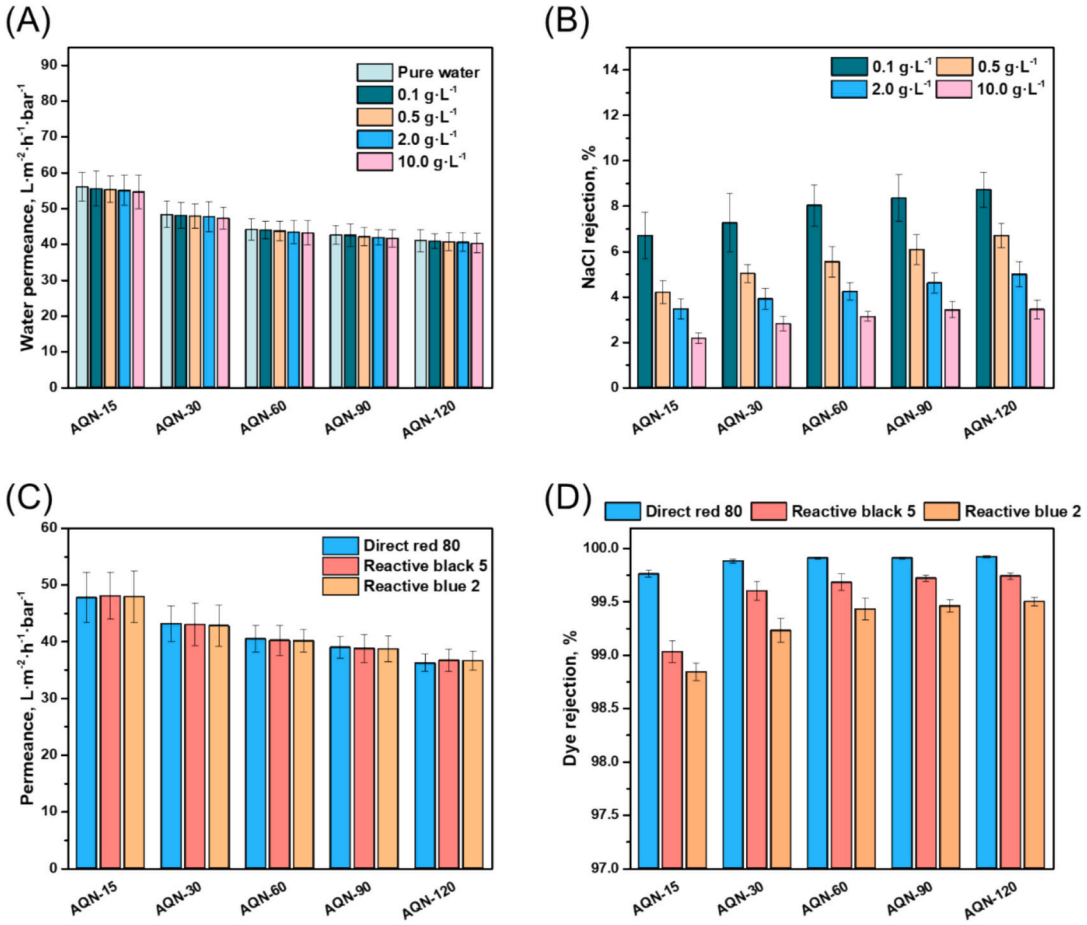

Fig. 7. Filtration performance of the fabricated AQN-coated tight ultrafiltration membranes in different concentrations of NaCl solutions (A, B) and various pure dye solutions (C, D).

tight ultrafiltration membranes showed a prominent improvement, particularly when the coating duration was extended from 30 min to 60 min. The dye rejection rates of the AQN-60 composite membrane for direct red 80, reactive black 5 and reactive blue 2 reached 99.91 %, 99.68 % and 99.43 %, respectively. Notably, the highest rejection of direct red 80 was attained by the membranes compared with the other dyes, i.e., reactive black 5 and reactive blue 2, since direct red 80 has a considerable geometric size and a high degree of aggregation for an enhanced size-sieving effect.

3.6.2. *Selective separation of dyes and salts*

The fractionation behavior of the prepared AQN-60 composite membrane was systematically evaluated via the filtration of dye/salt mixtures at different salt concentrations. As shown in Fig. 8, increasing

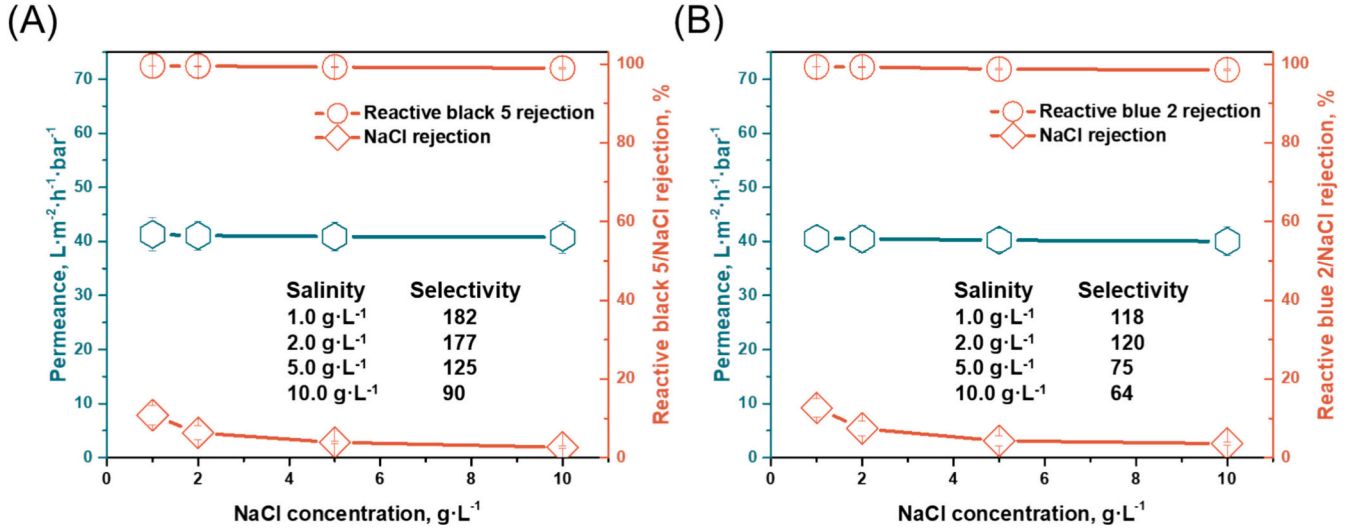

Fig. 8. Separation performance of the fabricated AQN-60 composite membrane for the reactive black 5/NaCl mixture (A) and the reactive blue 2/NaCl mixture (B).

salinity slowed the water permeance due to increasing osmotic pressure, as reflected by the minimal permeance decrease from 41.31 to 40.77 $L{\cdot}m^{-2}{\cdot}h^{-1}{\cdot}bar^{-1}$ and 40.56 to 40.03 $L{\cdot}m^{-2}{\cdot}h^{-1}{\cdot}bar^{-1}$ for the reactive black 5/NaCl mixture and BR2/NaCl mixture, respectively. Moreover, the retention of the AQN-60 composite membrane for dye and inorganic salts was also affected by the salinity of the feed solution. For the reactive black 5/NaCl mixture, the reactive black 5 rejection slightly decreased from 99.51 % to 98.92 %, whereas the NaCl rejection decreased from 10.78 % to 2.65 % when the salinity was increased to 10 $g{\cdot}L^{-1}$. A similar trend for dye and salt rejection was observed for the reactive blue 2/NaCl mixture. This phenomenon in solute rejection is attributed to the combined mechanisms of the "salting-out" effect and "charge shielding" effect. On the one hand, the presence of large amounts of inorganic salts exacerbated the dehydration of solute molecules by strongly attracting bound water, resulting in a decreased effective volume, which compromised the size exclusion of the membrane during filtration [16,42]. On the other hand, the increased ionic strength suppressed the Debye screening length of the membrane, thereby diminishing the electrostatic repulsion between the membrane and the charged dye molecules [43]. Overall, the AQN-coated membrane exhibited remarkable selectivity for dye/salt mixtures while maintaining moderate permeance at varying salinities, which demonstrated the great potential of the AQN-coated composite membrane for the efficient treatment of highly saline textile wastewater in terms of resource recovery.

3.6.3. *Long-term stability of the AQN-coated tight ultrafiltration membrane*

The long-term stability of the prepared AQN-60 composite membrane was assessed via 24-h continuous filtration with the reactive blue 2/NaCl mixture as the feed (Fig. 9). As shown in Fig. 9, the permeance of the AQN-60 composite membrane decreased markedly during the initial stage of filtration and then appeared to gradually plateau, with the permeance stabilizing at a level of ca. 34.5 $L{\cdot}m^{-2}{\cdot}h^{-1}{\cdot}bar^{-1}$. The sharp drop in permeance during the early filtration stage was likely attributed to membrane fouling from the accumulation of a dye cake layer, which increased the mass transfer resistance. Nevertheless, the increased surface hydrophilicity facilitated the formation of a hydration layer on the membrane surface, which served as a barrier to prevent dye penetration into the pores. As a result, the improved anti-fouling performance of the AQN-60 composite membrane ensured stable water permeance as the filtration operation progressed. In addition, the AQN-60 composite membrane exhibited stable rejection of both reactive blue 2 and NaCl throughout the 24-h operation. NaCl rejection remained consistently low at approximately 3.98 %, whereas reactive blue 2 rejection was maintained at a high level of 98.70 %. On the hand, the normalized flux of the AQN-coated membrane after 24-h filtration of a dye/salt mixture ultimately remained at the level of 87.9 %, indicating that the membranes maintained high permeance with minimal flux decline (by 12.1 %) and showed excellent resistance to fouling over time. This result demonstrates the superior long-term stability, durability and practicability of the AQN-coated membrane for the fractionation of dye and salt, guaranteeing sustainable management of highly saline textile wastewater.

3.7. *Antibacterial properties of the membranes*

Biofouling, a prevalent form of membrane fouling, is caused primarily by the accumulation of microorganisms on membrane surfaces. The limited antibacterial capacity and poor hydrophilicity of conventional membranes promote the formation of dense biofilms, which obstruct pores and reduce the productivity of the membrane system. To mitigate this issue, the natural antibacterial polypeptide ε-polylysine was introduced onto the membrane surface to increase its bactericidal ability (Fig. 10). As shown in Fig. 10, the pristine PES substrate demonstrated a weak biocide capacity against *E. coli*, as reflected by the extensive survival of *E. coli* colonies. In contrast, the AQN-60 composite membrane displayed excellent bacterial inhibition activity, with a high antibacterial rate of 98.75 % against *E. coli*. This remarkable antibacterial performance indicated the effectiveness of the AQN coating in preventing bacterial growth on the basis of the strong broad-spectrum antimicrobial activity of ε-polylysine, which can potentially mitigate membrane biofouling and extend the membrane lifespan in practical applications.

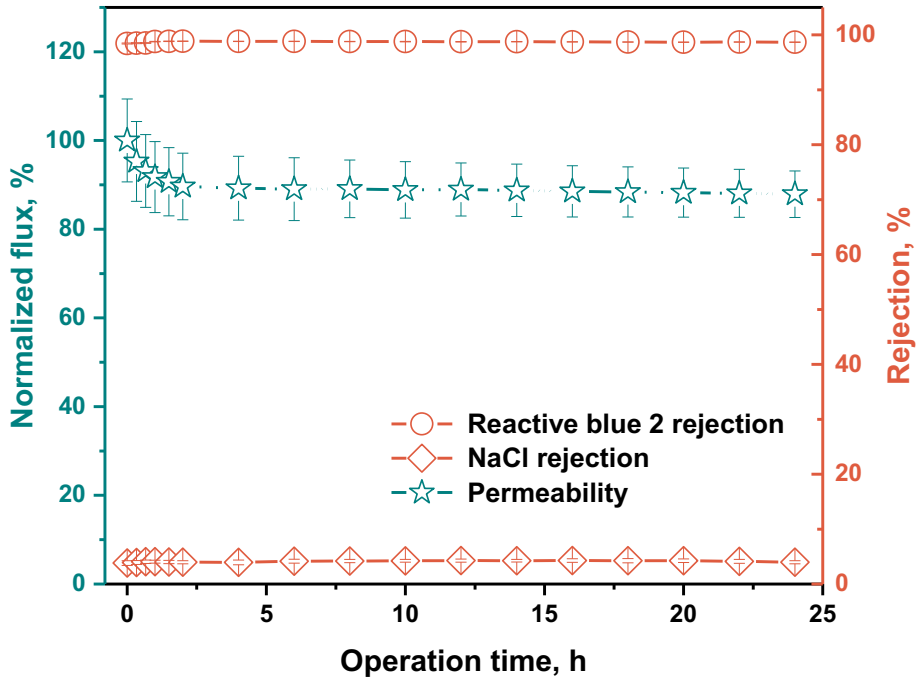

Fig. 9. Normalized flux and solute rejection as a function of operation time during a 24-h dye/salt mixed solution filtering experiment for the AQN-60 composite membrane.

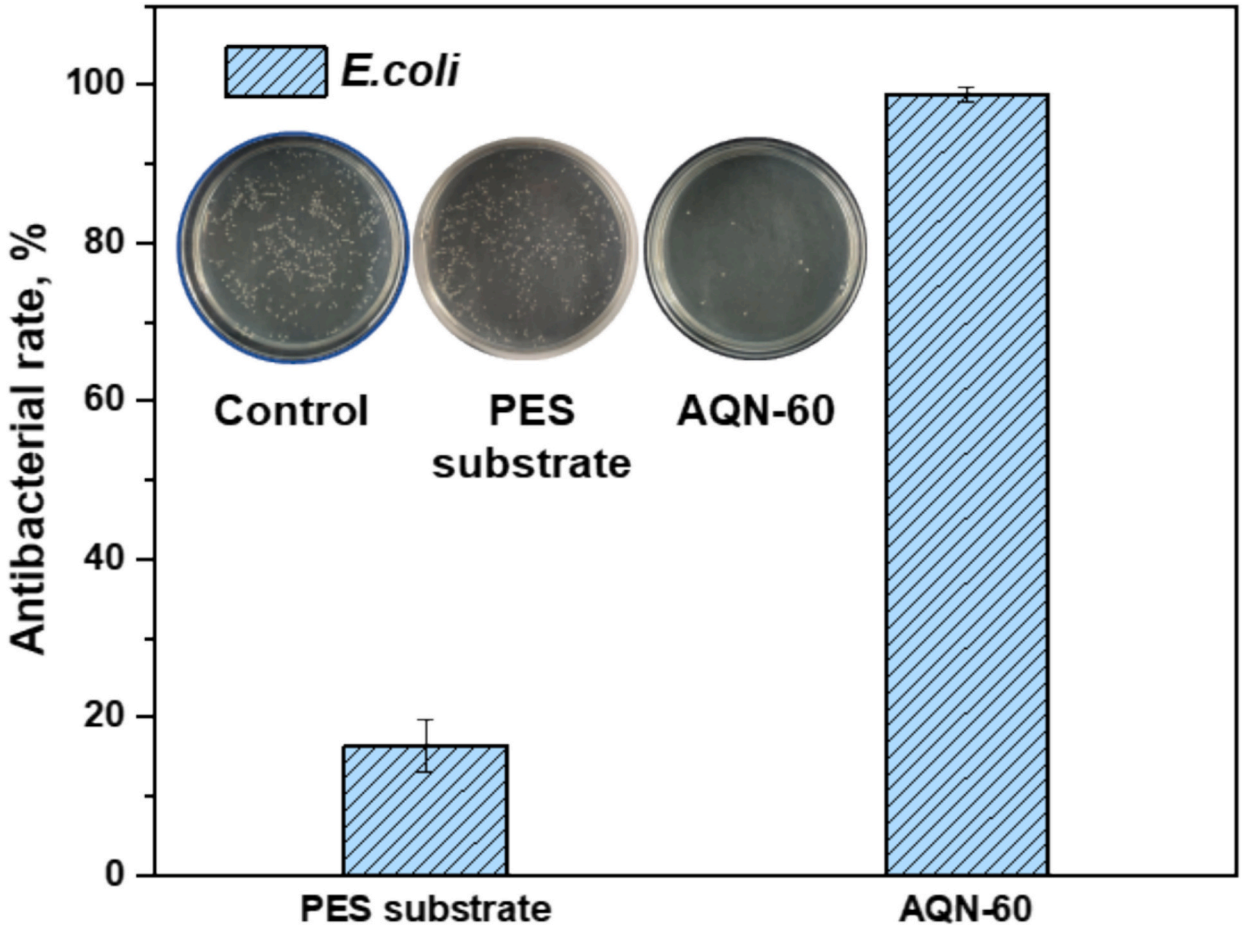

Fig. 10. The antibacterial performance of the pristine PES substrate and the prepared AQN-60 composite membrane.

4. Conclusion

In this study, dual-functional tight ultrafiltration membranes with high dye/salt selectivity and strong antibacterial properties were successfully constructed via the assembly of VA/ε-pl-based aminoquinone networks on a porous PES substrate. The surface properties, i.e., coating thickness, roughness, hydrophilicity and pore size, were effectively optimized by regulating the co-assembly duration of the aminoquinone networks. The optimal composite membrane (AQN-60) with an MWCO of 3450 Da yielded >98.50 % dye rejection and <3.56 % NaCl retention with comparable permeance even at a high salinity of 10.0 $g{\cdot}L^{-1}$, demonstrating its superior fractionation performance for dyes and salts. Furthermore, the AQN-60 composite membrane exhibited excellent long-term stability during a continuous 24-h filtration process of a reactive blue 2/NaCl mixture, with minimal flux reduction of 12.1 % for stable fractionation of dye and salt, due to the outstanding anti-fouling properties and durability of VA/ε-pl-based aminoquinone composite networks. In addition, the incorporation of the VA/ε-pl AQN composite coating endowed the membrane with superior antibacterial properties, with 98.75 % inhibition efficiency against *E. coli*, strengthening the practical application of the composite membrane in harsh environment. This study represents a novel strategy for designing high-performance and antibacterial tight ultrafiltration membranes, offering a technology platform for the sustainable management of highly saline textile wastewater.

Declaration of competing interest

The authors declare that they have no known competing financial interests or personal relationships that could have appeared to influence the work reported in this paper.

Acknowledgments

R. Liu acknowledges the support provided by the China Scholarship Council of the Ministry of Education (CSC No. 202106650001). J. Lin thanks the support from the Natural Science Foundation of Jiangxi Province (Grant No.: 20242BAB23019).

References

[1] J. Lin, W. Ye, M. Xie, D.H. Seo, J. Luo, Y. Wan, B. Van der Bruggen, Environmental impacts and remediation of dye-containing wastewater, Nat. Rev. Earth Env. 4 (2023) 785–803.
[2] D. Xu, H. Liang, X. Zhu, L. Yang, X. Luo, Y. Guo, Y. Liu, L. Bai, G. Li, X. Tang, Metal-polyphenol dual crosslinked graphene oxide membrane for desalination of textile wastewater, Desalination 487 (2020) 114503.
[3] J. Zheng, R. Zhao, A.A. Uliana, Y. Liu, D. de Donnea, X. Zhang, D. Xu, Q. Gao, P. Jin, Y. Liu, Separation of textile wastewater using a highly permeable resveratrol-based loose nanofiltration membrane with excellent anti-fouling performance, Chem. Eng. J. 434 (2022) 134705.
[4] W. Ye, F. Yu, Z. Yu, N. Kong, X. Lin, R. Liu, J. Du, X. Huang, A. Gu, S. Arcadio, High-performance antibacterial tight ultrafiltration membrane constructed by co-deposition of dopamine and tobramycin for sustainable high-salinity textile wastewater management, Desalination 579 (2024) 117482.
[5] S. Xie, Z. Yu, L. Chen, J. Du, J. Li, W. Yuan, X. Li, J. Lin, Thin-film composite electro-nanofiltration membrane for one-step and efficient fractionation of dyes and salts in high-salinity textile wastewater, Desalination 591 (2024) 118056.
[6] L. Zhang, L. Xu, H. Yu, P. Yao, M. Zhang, F. Guo, L. Yu, Capsaicin mimic-polyethyleneimine crosslinked antifouling loose nanofiltration membrane for effective dye/salt wastewater treatment, J. Membr. Sci. 641 (2022) 119923.
[7] J. Lin, Q. Chen, X. Huang, Z. Yan, X. Lin, W. Ye, S. Arcadio, P. Luis, J. Bi, B. Van der Bruggen, Integrated loose nanofiltration-electrodialysis process for sustainable

resource extraction from high-salinity textile wastewater, J. Hazard. Mater. 419 (2021) 126505.
[8] H.F.M. Austria, J.O. Young, O. Setiawan, T.-H. Huang, A.R. Caparanga, K.R. S. Pamintuan, W.-S. Hung, Thin film nanocomposite loose nanofiltration membranes with graphene oxide interlayer for textile wastewater treatment, Sep. Purif. Technol. 354 (2025) 129053.
[9] W. Gai, S. Hu, Z. Li, G. Dong, X. Pan, C. Li, S. Xu, J. Pan, Facilely prepare ultra-high molecular weight polypropylene loose nanofiltration membrane for efficient dye/salt separation, Desalination 587 (2024) 117928.
[10] Z.G. Abdi, J.-Y. Lai, T.-S. Chung, Green modification of P84 co-polyimide with β-cyclodextrin for separation of dye/salt mixtures, Desalination 549 (2023) 116365.
[11] P. Kumar, U.G. Thummar, N.H. Nandha, P.S. Singh, Sustainable treatment of saline dye wastewater and resource recovery with flux-recoverable hollow fiber of antifouling 'water channel', Desalination 549 (2023) 116308.
[12] U.S. Joshi, Anuradha, S.K. Jewrajka, Tight ultrafiltration and loose nanofiltration membranes by concentration polarization-driven fast layer-by-layer self-assembly for fractionation of dye/salt, J. Membr. Sci. 669 (2023) 121286.
[13] J. Lin, C.Y. Tang, W. Ye, S.-P. Sun, S.H. Hamdan, A. Volodin, C. Van Haesendonck, A. Sotto, P. Luis, B. Van der Bruggen, Unraveling flux behavior of superhydrophilic loose nanofiltration membranes during textile wastewater treatment, J. Membr. Sci. 493 (2015) 690–702.
[14] Y. Liu, G. Van Eygen, S. Yuan, H. Wang, M. Chi, D. Xu, Q. Gao, G. Li, J. Zheng, B. Van der Bruggen, Facile and novel fabrication of high-performance loose nanofiltration membranes for textile wastewater recovery, Sep. Purif. Technol. 308 (2023) 122867.
[15] Q.H. Shi, N. Zhang, D. Wang, J.J. Zhang, Y.M. Li, Z.N. Wang, Polyethylenimine-mica nanosheets/cellulose nanofibers stacked loose nanofiltration membrane for effective dye/salt separation, Desalination 551 (2023) 116410.
[16] Y. Zhao, Y. Liao, G.S. Lai, Y. Yin, R. Wang, A tight polyethersulfone ultrafiltration membrane fabricated via polyion complex assisted phase inversion for dye desalination, J. Membr. Sci. 685 (2023) 121908.
[17] U.S. Joshi, S. Samanta, S.K. Jewrajka, Low fouling polyelectrolyte layer-by-layer self-assembled membrane for high performance dye/salt fractionation: sequence effect of self-assembly, ACS Appl. Mater. Interfaces 16 (2024) 32748–32761.
[18] Anuradha, U.S. Joshi, S.K. Jewrajka, Low fouling molecular selective channels through self-assembly of cross-linked block copolymer micelles for selective separation of dye and salt, ACS Appl. Mater. Interfaces 16 (2024) 61344–61359.
[19] J. Lin, W. Ye, M.-C. Baltaru, Y.P. Tang, N.J. Bernstein, P. Gao, S. Balta, M. Vlad, A. Volodin, A. Sotto, Tight ultrafiltration membranes for enhanced separation of dyes and Na_2SO_4 during textile wastewater treatment, J. Membr. Sci. 514 (2016) 217–228.
[20] W. Ye, K. Ye, F. Lin, H. Liu, M. Jiang, J. Wang, R. Liu, J. Lin, Enhanced fractionation of dye/salt mixtures by tight ultrafiltration membranes via fast bio-inspired co-deposition for sustainable textile wastewater management, Chem. Eng. J. 379 (2020) 122321.
[21] M. Hu, S. Yang, X. Liu, R. Tao, Z. Cui, C. Matindi, W. Shi, R. Chu, X. Ma, K. Fang, Selective separation of dye and salt by PES/SPSf tight ultrafiltration membrane: roles of size sieving and charge effect, Sep. Purif. Technol. 266 (2021) 118587.
[22] B. Tansel, W. Bao, I. Tansel, Characterization of fouling kinetics in ultrafiltration systems by resistances in series model, Desalination 129 (2000) 7–14.
[23] N.-J. Lin, H.-S. Yang, Y. Chang, K.-L. Tung, W.-H. Chen, H.-W. Cheng, S.-W. Hsiao, P. Aimar, K. Yamamoto, J.-Y. Lai, Surface self-assembled PEGylation of fluoro-based PVDF membranes via hydrophobic-driven copolymer anchoring for ultra-stable biofouling resistance, Langmuir 29 (2013) 10183–10193.
[24] F. Qu, H. Liang, J. Zhou, J. Nan, S. Shao, J. Zhang, G. Li, Ultrafiltration membrane fouling caused by extracellular organic matter (EOM) from *Microcystis aeruginosa*: effects of membrane pore size and surface hydrophobicity, J. Membr. Sci. 449 (2014) 58–66.
[25] J. Zhu, J. Hou, Y. Zhang, M. Tian, T. He, J. Liu, V. Chen, Polymeric antimicrobial membranes enabled by nanomaterials for water treatment, J. Membr. Sci. 550 (2018) 173–197.
[26] L. Ren, J. Chen, Q. Lu, J. Han, H. Wu, Anti-biofouling nanofiltration membrane constructed by in-situ photo-grafting bactericidal and hydrophilic polymers, J. Membr. Sci. 617 (2021) 118658.
[27] J. Sun, B. Zhang, B. Yu, B. Ma, C. Hu, M. Ulbricht, J. Qu, Maintaining antibacterial activity against biofouling using a quaternary ammonium membrane coupling with electrorepulsion, Environ. Sci. Technol. 57 (2023) 1520–1528.
[28] L. Xu, Z. Pang, H. Yu, M. Guo, X. Yan, X. Jiang, L. Yu, Antifouling loose nanofiltration membranes prepared via the fast codeposition of capsaicin-mimic/polydopamine for efficient dye/salt separation, Desalination 565 (2023) 116809.
[29] Q.Z. Zhong, J.J. Richardson, A. He, T. Zheng, R.P. Lafleur, J. Li, W.Z. Qiu, D. Furtado, S. Pan, Z.K. Xu, Engineered coatings via the assembly of amino-quinone networks, Angew. Chem. 133 (2021) 2376–2384.
[30] J. Song, D. Xu, X. Luo, Y. Han, J. Ding, X. Zhu, L. Yang, G. Li, H. Liang, In-situ assembled amino-quinone network of nanofiltration membrane for simultaneously enhanced trace organic contaminants separation and antifouling properties, J. Membr. Sci. 661 (2022) 120891.
[31] T. Gao, P. Fu, W.-L. Li, W.-T. Lin, Y.-H. Yu, X.-J. Huang, Z.-K. Xu, L.-S. Wan, Positively charged loose nanofiltration membranes via the assembly of amino-quinone networks for efficient dye/salt separation, Desalination 117794 (2024).
[32] W. Cheng, Y. Yu, W. Liu, X. Wang, M. Zhou, B. Xu, P. Wang, Q. Wang, Self-assembly amino-quinone network coatings onto polyester fabric via single-sided spraying of natural polyphenols and polyethyleneimine for highly efficient moisture conducting and bacteriostatic properties, Appl. Surf. Sci. 606 (2022) 154913.
[33] T. Gao, P. Fu, W.-L. Li, W.-T. Lin, Y.-H. Yu, X.-J. Huang, Z.-K. Xu, L.-S. Wan, Positively charged loose nanofiltration membranes via the assembly of amino-quinone networks for efficient dye/salt separation, Desalination 586 (2024) 117794.
[34] M. Yan, M. Shao, J. Li, N. Jiang, Y. Hu, W. Zeng, M. Huang, Antifouling forward osmosis membranes by ε-polylysine mediated molecular grafting for printing and dyeing wastewater: preparation, characterization, and performance, J. Membr. Sci. 668 (2023) 121288.
[35] D.Y. Kim, J. Lee, H. Park, S.-J. Park, J.-H. Lee, Ecofriendly hydrophilic modification of microfiltration membranes using pyrogallol/ε-polylysine, Separ. Purif. Technol. 350 (2024) 127988.
[36] R. Ye, H. Xu, C. Wan, S. Peng, L. Wang, H. Xu, Z.P. Aguilar, Y. Xiong, Z. Zeng, H. Wei, Antibacterial activity and mechanism of action of ε-poly-L-lysine, Biochem. Biophys. Res. Commun. 439 (2013) 148–153.
[37] N. Zhang, B. Jiang, L. Zhang, Z. Huang, Y. Sun, Y. Zong, H. Zhang, Low-pressure electroneutral loose nanofiltration membranes with polyphenol-inspired coatings for effective dye/divalent salt separation, Chem. Eng. J. 359 (2019) 1442–1452.
[38] Q. Wei, F. Zhang, J. Li, B. Li, C. Zhao, Oxidant-induced dopamine polymerization for multifunctional coatings, Polym. Chem. 1 (2010) 1430–1433.
[39] D. Liu, Y. Chen, T.T. Tran, G. Zhang, Facile and rapid assembly of high-performance tannic acid thin-film nanofiltration membranes via Fe^{3+} intermediated regulation and coordination, Sep. Purif. Technol. 260 (2021) 118228.
[40] G.P. Abatti, A.T.N. Pires, A. Spinelli, N. Scharnagl, T.F. da Conceição, Conversion coating on magnesium alloy sheet (AZ31) by vanillic acid treatment: preparation, characterization and corrosion behavior, J. Alloys Compd. 738 (2018) 224–232.
[41] R. Liu, Q. Chen, M. Cao, J. Lin, F. Lin, W. Ye, P. Luis, B. Van der Bruggen, S. Zhao, Robust bio-inspired superhydrophilic and underwater superoleophobic membranes for simultaneously fast water and oil recovery, J. Membr. Sci. 623 (2021) 119041.
[42] J. Luo, Y. Wan, Effects of pH and salt on nanofiltration—a critical review, J. Membr. Sci. 438 (2013) 18–28.
[43] M. Jiang, K. Ye, J. Deng, J. Lin, W. Ye, S. Zhao, B. Van der Bruggen, Conventional ultrafiltration as effective strategy for dye/salt fractionation in textile wastewater treatment, Environ. Sci. Technol. 52 (2018) 10698–10708.